Available online at www.sciencedirect.com
ScienceDirect
Journal of Nuclear Materials 362 (2007) 327–335
journal of nuclear materials
www.elsevier.com/locate/jnucmat

Mechanistic modelling of urania fuel evolution and fission product migration during irradiation and heating

M.S. Veshchunov [a], R. Dubourg [b,*], V.D. Ozrin [a], V.E. Shestak [a], V.I. Tarasov [a]

[a] Nuclear Safety Institute of the Russian Academy of Sciences (IBRAE), Moscow, Russia
[b] Institut de Radioprotection et de Sûreté Nucléaire (IRSN), DPAM SEMIC LEPF, St Paul lez-Durance, France

Abstract

The models of the mechanistic code MFPR (Module for Fission Product Release) developed by IBRAE in collaboration with IRSN are described briefly in the first part of the paper. The influence of microscopic defects in the UO_2 crystal structure on fission-gas transport out of grains and release from fuel pellets is described. These defects include point defects such as vacancies, interstitials and fission atoms, and extended defects such as bubbles, pores and dislocations. The mechanistic description of chemically active elements behaviour (fission-induced) is based on complex association of diffusion–vaporisation mechanism involving multi-phase and multi-component thermo-chemical equilibrium at the grain boundary with accurate calculation of fuel oxidation. In the second part, results of the code applications are given to different situations: normal LWR reactor operation, high temperature annealing, loss of coolant accident (LOCA) and severe accidents conditions.

1. Introduction

The MFPR code (Module for Fission Product Release), currently being developed by IBRAE (Moscow) in collaboration with IRSN (Cadarache, France), describes mechanistically the fission product (FP) behaviour in intact UO_2 fuel under irradiation regimes, annealing regimes and accidental situations [1]. As a first objective, the code is used for interpretation of complex large scale [2] or semi analytical experiments [3], but is also used for benchmarking of more simplified reactor code models and could be part of a fuel performance code in near future. It is extensively validated against separate-effect tests, semi-analytical out-of-pile tests and large scale in-pile tests. Trying to avoid any arbitrary tuning, the code self-consistently describes evolution of the fuel microstructure and various defects interactions with gaseous fission products. The parameters characterizing the crystal defect structure naturally arise and are determined from available analytical experimental data.

In addition, as shown by many observations, the release of various chemically-active fission products strongly depends on formation and thermal behaviour of separate phases in various gas atmospheres. Indeed, the stability of these phases is associated

* Corresponding author. Tel.: +33 4 42199502; fax: +33 4 42199167.
E-mail address: roland.dubourg@irsn.fr (R. Dubourg).

0022-3115/$ - see front matter © 2007 Elsevier B.V. All rights reserved.
doi:10.1016/j.jnucmat.2007.01.081

with the fuel oxygen potential. MFPR includes detailed modelling of chemistry of FP's within irradiated oxide fuel at high temperatures in the range 500–3000 K.

Models of the code were described in detail in [1] and the present paper will overview them, better focusing on examples of validation of individual models against separate-effects experiments and results of applications in the case of normal LWR reactor irradiation conditions, high temperature annealing, loss of coolant accident (LOCA) and severe accidents situations.

2. Physical processes and models

It is assumed that FP elements are originally generated in the UO_2 matrix in atomic (or ionic) form. All atoms formed by fission processes migrate to grain boundaries. In this way, fission gas atoms can form intragranular gas bubbles in which they might be further trapped. These bubbles can also migrate to grain boundaries. Part of the captured atoms can escape from bubbles by irradiation-induced and thermal re-solution processes.

Chemical interactions between the FP elements and the dissolved oxygen result in formation of separate phases in solid precipitates on the grain boundaries and vaporisation to the intergranular gas bubbles considered as the major mechanism for release of the fission products. Since distribution of elements depends significantly on the oxygen potential of the system, a model for fuel oxidation in steam/air mixtures was also developed. Processes of vapour formation affect significantly the release rates of all FP elements including noble gases.

In MFPR, intergranular bubbles are represented by three groups: bubbles on grain faces (GF), on grain edges (GE) and in grain corners (GC). The GF bubble growth progresses up to the grain surface saturation, when interlinkage of the GF bubble and formation of grain face channels to the grain edges and corners occurs. Growth of the GE and GC bubbles leads to their interconnection by tunnels and formation of an open porosity structure.

2.1. Intragranular transport of FP elements

In the transport problem, a fuel grain is considered for simplicity as an isotropic sphere (of radius R_{gr}).

2.1.1. Diffusion and release of chemically active FP elements

In the MFPR chemistry model, irradiated oxide fuel including fission products and dissolved oxygen is considered as a multiphase system consisting of multi-component phases. The list of FP elements considered in the model consists of Sr, Zr, Nb, Mo, Ru, Sb, Te, I, Xe, Cs, Ba, La, Ce, Nd and Eu. According to experimental data [4] and thermo-chemical calculations [5–8], the phases considered in the model are the solid solution of FP elements and oxygen in UO_2 matrix, the metal phase consisting of Mo and Ru, the oxide phase of complex ternary compounds including molybdates, zirconates and uranates of Cs, Ba and Sr, the solid phase of CsI and the gas phase. Formulation of the model is based on the following simplifying assumptions:

- Fission product elements migrate within the UO_2 matrix in the atomic form, capturing of FP elements (except Xe) by intragranular bubbles is not considered. Chemical interactions which could result in formation of the FP oxides contribute to the diffusion coefficients and concentration of the dissolved oxygen.
- Since the coefficient of solid state diffusion of oxygen is significantly higher than that of the fission product elements, the dissolved oxygen being in the local equilibrium with FP elements and oxides in the matrix has a spatially homogeneous concentration.
- Separate solid phases (precipitates) are formed only at the gas/solid interface. Possibility of existence of such phase inclusions within the matrix (or anywhere else in the fuel) is not taken into account. It is assumed that existence of these phases is determined by thermodynamic conditions only. Kinetic limitations on formation of solid phases or on vapour formation are ignored.
- Subsystem including the gas phase (intergranular bubbles) and solid precipitates (SP/G) is in the equilibrium state, and it is in equilibrium with the boundary layer of solid solution.

To formulate the transport problem, the complex system is separated into two subsystems. That is (1) solid solution (SS) of FP elements, their oxides and atomic oxygen dissolved in the UO_2 matrix, and (2) the subsystem 'solid precipitates–gas phase' (SP/G) including the white and 'grey' phases and the phase of condensed CsI(c). Concentration profiles of FP

elements in SS are described by simple diffusion equations, without any trapping because separate phases are present only at grain boundaries:

$$\frac{\partial}{\partial t} C_i^{(1)} = B_i + r^{-2} \frac{\partial}{\partial r} \left(D_i r^2 \frac{\partial}{\partial r} C_i^{(1)} \right), \tag{1}$$

where $C_i^{(1)}$ is the local volume concentration of the ith element in the subsystem 1 – solid solution, B_i is the build-up rate of the ith element due to fission, D_i is its diffusion coefficient. Boundary conditions for these equations are determined by the thermochemical equilibrium within the SP/G subsystem and at the subsystem interface, which depends on fluxes of elements out of SS. The problems of FP transport and the phase formation are solved self-consistently with the problem of fuel oxidation. The equilibrium composition of the phases is treated in terms of semi-ideal chemistry model in which phenomenological solid solubilities of FP elements are used, and the chemical potential of dissolved oxygen is described by the Lindemer–Besmann correlation [9].

2.1.2. Transport of fission gas

The basic space-time dependent variables are the volume concentrations of gas atoms C_g and bubbles C_b, the average number of gas atoms within a bubble N_b, and the average bubble volume V_b.

Additionally, MFPR includes self-consistent consideration of point defects (vacancies and interstitials) and dislocations, which mutually interact with each other and with gas bubbles and as-fabricated pores during their evolution under irradiation or annealing conditions. These defects are described by three additional variables: vacancy concentration C_v, interstitial concentration C_i, dislocation density (length per unit volume) ρ_d, and concentration of atoms captured by dislocations Y_d.

Transport equations for C_g and concentration of atoms-in-bubbles $Y_b = N_b C_b$ can be written as

$$\frac{\partial C_g}{\partial t} = D_g \Delta C_g - F_{g\to b} - F_{g\to d} + \kappa G, \tag{2}$$

$$\frac{\partial Y_b}{\partial t} = \nabla (D_b \nabla Y_b) - \omega_{bmg} Y_b + F_{g\to b} - F_{b\to d}, \tag{3}$$

where

$$F_{g\to b} = k_{gg} F_n C_g^2 + k_{gb}(C_g - C_g^{eq}) C_b - bGY_b, \qquad k_{xy} = 4\pi (D_x + D_y)(R_x + R_y), \quad x, y = g, b \tag{4}$$

with boundary conditions formulated in [1].

Different terms in the right hand side of these equations correspond to the following physical effects, each being characterized by a particular kinetic parameter:

- Diffusion (D_g and D_b are the diffusivities of gas atoms and bubbles, respectively).
- Gas atom generation by fission (G is the fission rate and κ is the probability of Xe formation by fission).
- Bubble biased migration (ω_{bmg}) along the temperature gradient.
- Bubble nucleation (with the nucleation rate F_n).
- Gas atom capture by bubbles (R_g is the gas-atom radius and R_b is the bubble radius in the capture kernel k_{gb}).
- Thermal re-solution ($C_g^{eq} = PK_S\varphi(P,T)$) is the equilibrium concentration of non-ideal gas with parameters specified in [1].
- Radiation induced re-solution (b is the re-solution probability factor).

Modelling of these effects as well as sweeping of gas and bubbles by climbing dislocations, $F_{g\to d}$ and $F_{b\to d}$ (which are currently considered only in annealing conditions) are described in [1]. Superposition of these effects (along with the Van-der-Waals equation for the gas state) determines, in particular, the intragranular bubbles concentration C_b and mean radius R_b, as well as gas release to the grain faces.

In growing grains, the boundary conditions of Eqs. (2) and (3) are set at moving grain boundaries. A detailed description of the mechanistic grain growth kinetic models implemented in MFPR is given in [10].

2.1.3. Evolution of point defects in irradiated UO_2 fuel

In the mean field approximation [11], c_v and c_i (number of vacancies and interstitials per uranium atom) are expressed as

$$\dot{c}_v = -(k_v^2 + k_{vgb}^2) D_v c_v - \alpha D_i c_i c_v + K_e + K_b + K_p + (1-\xi)K, \tag{5}$$

$$\dot{c}_i = -(k_i^2 + k_{igb}^2) D_i c_i - \alpha D_i c_i c_v - K_d + K, \tag{6}$$

where D_v and D_i are the vacancy and interstitial diffusion coefficients, respectively; α is the recombination constant; k_v^2 and k_i^2 are the total sink strength of vacancies and interstitials into the extended defects (gas bubbles, pores, vacancy clusters and

dislocations), respectively; k^2_{vgb} and k^2_{igb} are the grain-boundary sink strength for vacancies and interstitials, respectively; K is the Frenkel pair production rate proportional to the fission rate G; ξK is the rate at which vacancies are removed from solution to form vacancy loops; K_e is the rate of the vacancy thermal production; K_p is the rate of the vacancy irradiation-induced re-solution (knock-out) from pores; K_b is the rate of the vacancy irradiation induced resolution from gas bubbles; K_d is the rate of the interstitial absorption due to the interstitial loop generation.

Each term of Eqs. (5) and (6) are described in [1,12]. The total sink strength of vacancies and interstitials due to the extended defects (bubbles, pores (C_p), dislocations, vacancy clusters (C_{vl})) are calculated as

$$k^2_{i,v} = 4\pi R_b C_b + 4\pi R_p C_p + Z_{i,v}(\rho_d + 2\pi R_l C_l + 2\pi R_{vl} C_{vl}). \quad (7)$$

The calculation of vacancy concentration has two main important consequences. First, this concentration determines the gas bubble nucleation factor $F_n = c_v$ leading to 'saturation' of the intragranular bubbles concentration at high burn-up, see Section 3.1. Second, it influences evolution of extended defects and relaxation kinetics of bubbles and pores. Details for evolution of extended defects are given in [1,12].

2.2. Intergranular transport of FP elements

2.2.1. Model of FP release by bubble interlinkage

The equations governing the FP transport from the intergranular bubbles to the open porosity are formulated based on a percolation type approach close to that developed by White and Tucker [13]. In the case of the grain face bubbles, the rate equation takes the form

$$\frac{d}{dt} C_f^{(i)} = F_f^{(i)} \theta_f, \quad \theta_f \equiv \theta(A^* - A_f), \quad (8)$$

where A_f is the projected area coverage of the grain face by the face bubbles, $\theta(x) = 1$ for $x > 0$ and $\theta(x) = 0$ for $x \leqslant 0$, and $F_f^{(i)}$ is the flux of gaseous species 'i' to the face bubbles. The critical area coverage of the grain face $A^* = 0.5$ determines the onset of formation of the grain-face interconnected channels to the grain edges.

The rate equations for the concentration of the gas component in the GE and GC bubbles have the form

$$\frac{d}{dt} C_e^{(i)} = F_e^{(i)} \theta_e, \quad \frac{d}{dt} C_c^{(i)} = F_c^{(i)} \theta_e, \quad (9)$$

where $F_e^{(i)}$ and $F_c^{(i)}$ are the gas fluxes to the grain edge and grain-corner bubbles, respectively; θ_e becomes equal to 0 when saturation of the grain edge and grain corner porosity takes place (i.e. when these bubbles are just touching each other). Finally, the release rate of the ith gas component is determined by

$$\frac{d}{dt} Y_{out}^{(i)} = \left[F_e^{(i)} + F_c^{(i)} + F_f^{(i)}(1 - \theta_f)\right](1 - \theta_e). \quad (10)$$

2.2.2. Xe grain face diffusion transport

An advanced model for the grain face transport based on the self-consistent consideration of gas atoms diffusion, sinking to and resolution from bubbles on grain faces, is developed and implemented in MFPR [1]. 'Circulation' of gas atoms collected by growing intergranular bubbles from the grain face and then returned back (by the re-solution process) into the grain matrix, makes intergranular bubbles much less effective sinks for gas atoms, since it decreases their growth (i.e. approaching a balance among absorbed and re-emitted atoms) and thus continuously increases a fraction of the source term flux (i.e. diffusion flux from grain to GF) eventually transported to grain edges. In particular, this allows prediction of a possible gas release from fuel when the grain-face coverage is far below the saturation value (at which interlinkage of face bubbles occurs), as observed in the tests [14].

2.2.3. Intergranular swelling model

Random migration of grain face bubbles is considered as the main mechanism of their coalescence. The coalescence frequency of bubbles randomly moving on a surface can be represented by the formula derived in [15]

$$\varpi_{cls} = \frac{8\pi D_{bf}}{\ln\left(\frac{D_b \tau_0}{2R_f^2}\right)} \approx 8\pi\chi D_{bf}, \quad (11)$$

where τ_0 is the characteristic time of the two-fold increase of the mean bubble radius R_f. Being a weak function of its argument (and thus, of R_f), logarithm can be approximated by a constant value, i.e. $\chi \approx$ const.

Face bubble diffusion coefficient D_{bf} depends on the dominating microscopic mechanism of bubble migration, with parameters fitted on data from the annealing tests [16].

3. Examples of applications of the MFPR code

MFPR code has been validated against a wide set of analytical tests including, in particular, VERCORS 1, 2, 4 and 5 tests using respectively oxidising and oxidising/reducing gas mixtures, and two groups of high-temperature tests from HI-VI series (ORNL), VI-1, VI-2, VI-3 and VI-4, VI-5, performed respectively in steam and hydrogen atmospheres. In this section, some MFPR applications are discussed.

3.1. Irradiation conditions

The code has been applied to experimental data [17,18]. In these experiments after reactor irradiation in a wide range of burn-ups (6–83 GW d t^{-1}), the characteristics of intra-granular bubbles and dislocations in UO_2 fuel pellets (middle part) were examined.

Calculations performed on these analytical results (Fig. 1) permitted to fit values of important microscopic parameters like the vacancy loop formation rate, the damage formation in fission tracks rate, the interstitial bias factor, the vacancy-interstitial recombination radius, which are further used without additional tuning.

The code was also used for calculation of intra/intergranular partition of fission gases after reactor operations for a high burn up fuel of about 60 GW d t^{-1}. In Table 1, we compare the results to the experimental data presented in details in [19]. Although the actual fuel conditions during reactor operations were only approximated in this calculation, the agreement is quite reasonable and further developments will permit to improve it concerning intragranular gas (interactions with dislocations) and intergranular gas by considering possible trapping of gas in remaining as-fabricated porosities or more accurate reproduction of thermo-mechanical behaviour of fuel during reactor operations, notably stresses exerted on it.

The code predicts a complete suppression of the intra-granular bubble nucleation at $T > 2273$ K, in a qualitative agreement with observations of [20], and a significant delay in the onset of the bubble formation at low temperatures $T < 973$ K, as

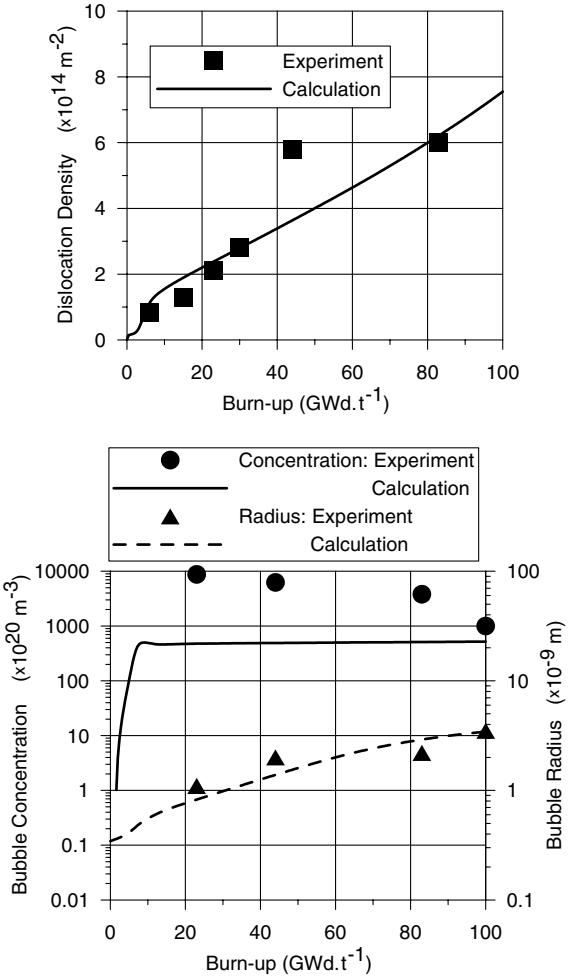

Fig. 1. Dislocations density, intra-granular bubbles concentration and bubble radius as a function of burn-up, calculated in steady state irradiation conditions at 900 K.

Table 1
Calculated fractions (in vol.%) of FP gas in different locations for two radial pellet zones of a high burnup fuel (60 GW d t^{-1})

Location	Intragranular	Intergranular	Released
Hot zone	79 (73)	8 (13)	13 (14)
Cold zone	80 (87)	9 (7)	11 (6)

Experimental values from [19] are given in brackets.

observed in tests [21], owing to the thermal re-solution effect presented in Eq. (4) by the term $k_{gb}(C_g - C_g^{eq})C_b$ (see [1]). The equilibrium gas concentration C_g^{eq} associated with finite Xe solubility in the fuel matrix exceeds the calculated steady state gas concentration C_g at high (>2300 K) and low (<1000 K) temperatures, as illustrated in Fig. 2,

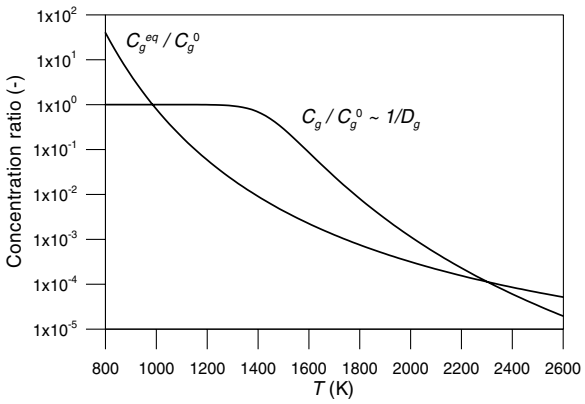

Fig. 2. Temperature dependence of the equilibrium gas concentration C_g^{eq} and the steady-state gas concentration C_g, normalized against the 'athermal' low temperature gas concentration C_g^0.

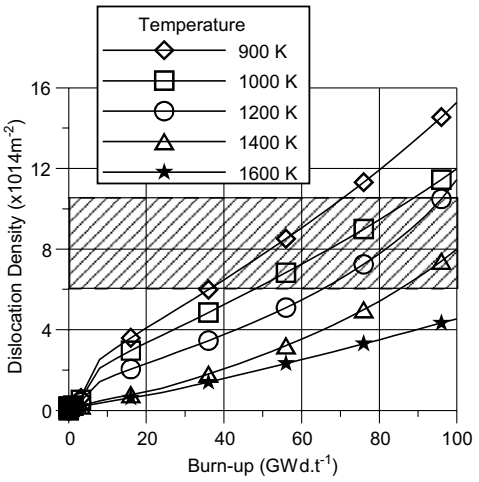

Fig. 3. Dislocations density as a function of burn-up, calculated in steady state irradiation conditions at different temperatures.

and thus results in suppression of bubble nucleation process.

3.1.1. Fuel restructuring at high burn-up

As observed in [17] at ≈900 K, tangled dislocation networks with low-angle grain boundaries were formed by accumulation of dislocations in the 44 GW d t^{-1} fuel, when dislocation density attained $\approx 6 \times 10^{14}$ m^{-2}. For the higher burnup fuel of 83 GW d t^{-1}, dislocations further accumulated and ultimately evolved into sub-divided grains with high-angle boundaries. The sub-divided grains with high-angle boundaries were postulated in [17] as the nucleus for the recrystallization of fuel.

This result well correlates with other observations of the burnup threshold between 55 and 82 GW d t^{-1} [22].

In accordance with the general theory of cell structure formation [23], dislocation structures tend to develop with increasing dislocation density and to form dislocation clusters in which neighbouring dislocations mutually screen their stress field. The cell structure terminates the structural evolution, when dislocation density attains a certain ultimate value.

From analysis of the above presented test observations [17], the transition from low-angle to large-angle cells occurs in the range of dislocation density from $\approx 6 \times 10^{14}$ to $\approx 10^{15}$ m^{-2}, Fig. 1. Application of these ultimate criteria to higher temperatures is presented in Fig. 3, where dislocation density evolution with burnup was calculated by the MFPR dislocation model (with microscopic parameters fixed from the analysis of the test [17]).

From these calculations it is seen that the temperature threshold at which no restructuring occurs, at least up to 100 GW d t^{-1}, is at 1300–1400 K, in a good agreement with various observations (see [22]).

3.2. Annealing regimes at high temperature

Under annealing conditions, non-stationary vacancy-diffusion problem in the grain is considered:

$$\frac{\partial c_v}{\partial t} = \frac{1}{r^2}\frac{\partial}{\partial r}\left(r^2 D_v \frac{\partial c_v}{\partial r}\right) - 4\pi D_v R_b C_b \left(c_v - c_v^{bs}\right) + \rho_d V_d b \tag{12}$$

with equilibrium conditions at the grain boundary, $c_V|_{r=R_{gr}} = c_V^{eq}$, and at the intragranular bubbles surfaces, $c_V^{bs} = c_V^{eq} \exp(-\Omega\delta p/kT)$.

The results of MFPR calculation of annealing tests [16] for a 25 GW d t^{-1} irradiated fuel are compared with experimental data in Fig. 4.

During initial period of the tests when active growth and coalescence of intragranular bubbles occur owing to gas atoms sinking, dislocation loops uniformly distributed in the grain bulk act as the main sources of vacancies (necessary for equilibration of growing bubbles). This explains dislocation creep (with velocity v_d) and enhanced bubble growth by dislocation sweeping under annealing conditions, observed in [24].

In this situation a new mechanism for gas release due to dislocation creep emerges [1,12]. This mechanism considers sweeping of bubbles and delivery

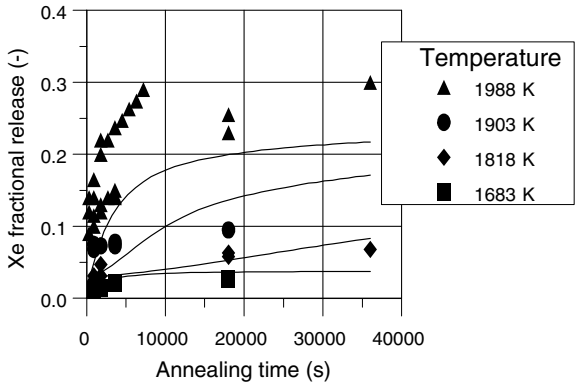

Fig. 4. Experimental data [16] (points) and MFPR calculation results (lines) for Xe release as a function of annealing time at different temperatures.

them to the grain boundaries by climbing dislocation segments in the course of vacancy generation. After some time, a strong pinning of dislocations by swept bubbles occurs, and grain boundaries apparently become the dominant source of vacancies during the subsequent period of the annealing tests. In this situation a vacancy flux directed from grain surface to its interior arises that induces bubble biased migration upward the vacancy gradient, $V_b^{vac}(r) = 2D_v\partial c_v/\partial r$, as proposed by Evans [25].

3.3. Gas behaviour in LOCA accident

The code was applied to the calculation of fission gas behaviour in LOCA transient for a standard PWR UO_2 pellet irradiated at 48.5 GW d t^{-1}. Experimental results are presented in [26] in detail. Calculations were performed with a simplified irradiation history and without consideration of stresses exerted on the fuel during the sequence. Even with these simplifications, the code gives rather encouraging results in Fig. 5.

Notably the code reproduces correctly observations of [26] that the gas release comes from intergranular gas accumulated during irradiation, Fig. 5. Underestimation of the release is associated with underestimation of initial intergranular content, mainly in the inner hot zone of the pellet (see Table 1). As shown in [26], stresses exerted on the fuel during the tests by the cladding noticeably influence the kinetic release. Preliminary calculations (not reproduced here) considering stresses during reactor operations show much better agreement with experiments.

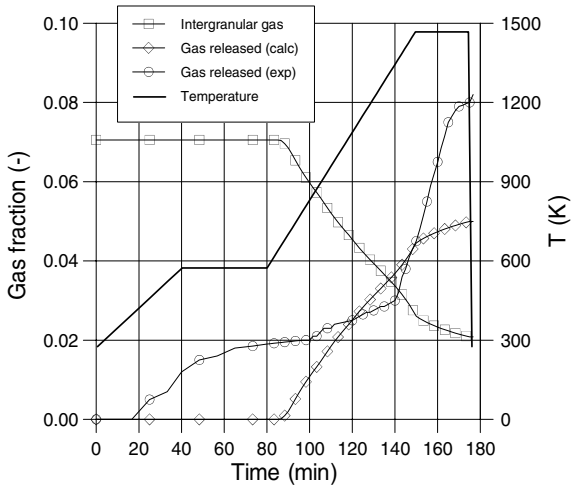

Fig. 5. Fission gas behaviour calculated by the MFPR code during a LOCA sequence for an irradiated fuel (48.5 GW d t^{-1}). Comparison with experimental data [26].

3.4. Fission product behaviour in severe accident

An illustration of one chemically active element behaviour under severe accident conditions is given, i.e. the behaviour of caesium in the VERCORS 4 test. This test from the French VERCORS program [3] was performed at high temperature and in pure hydrogen during the final part, after clad pre-oxidation in mixed atmosphere at an intermediate temperature plateau. Results of the MFPR code simulations are given in Figs. 6 and 7.

Fig. 6 shows that the calculated Cs release kinetic is in good agreement with experimental data.

Additionally, it is shown in Fig. 7 that the behaviour of Cs during the experiments is mainly associated with stability of the ternary compound (grey)

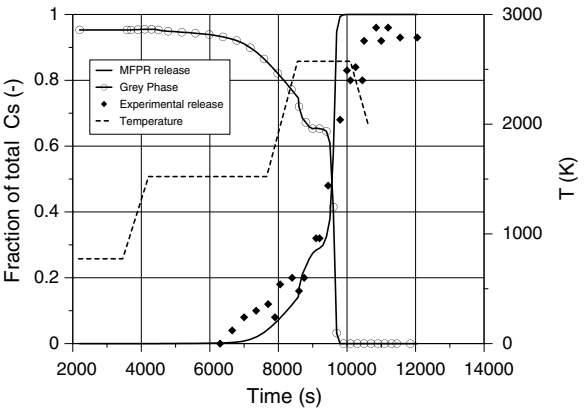

Fig. 6. Calculated Cs behaviour in VERCORS 4 as compared with experimental data for ^{137}Cs [3].

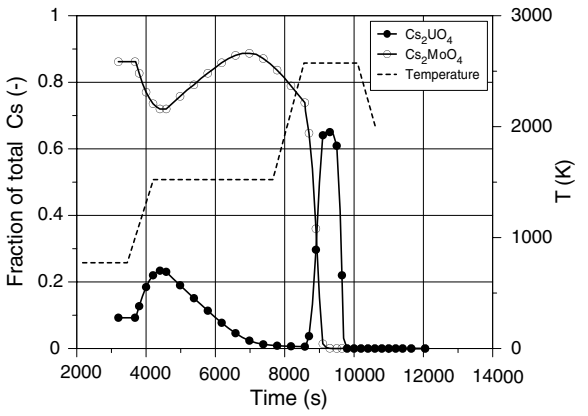

Fig. 7. Calculated behaviour of Cs ternary compounds in VERCORS 4.

phase. In particular, during the clad oxidation plateau (~4500–8500 s) some of the produced hydrogen reacts with the fuel, resulting in a partial Cs_2UO_4 destruction and Cs release. Then after complete clad oxidation the remaining injected steam interacts with fuel, producing some Cs_2MoO_4. In the final step of experiment, in a pure hydrogen atmosphere and at high temperature, Cs_2MoO_4 and the remaining part of Cs_2UO_4 become unstable, giving the final release.

Another illustration is given by the molybdenum behaviour reproduced by MFPR in typical severe accident situations as those of PHEBUS FP tests [2].

For the high elevation of the bundle, Fig. 8 shows that molybdenum is initially located in the metallic phase (along with Ru mainly) in which it remains

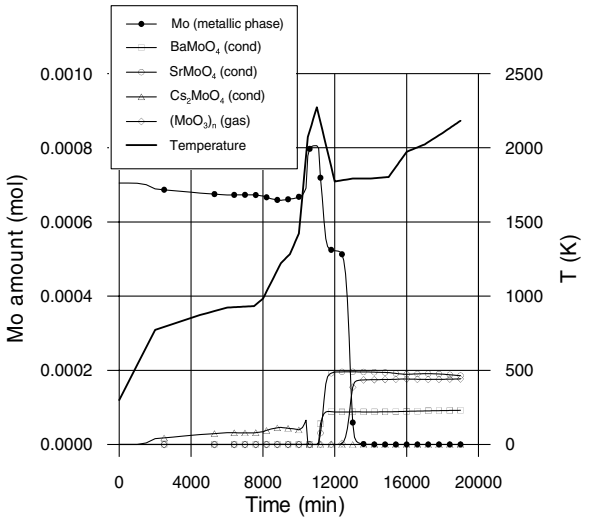

Fig. 8. Calculated behaviour of Mo in severe accident at high elevation in the bundle.

during the clad oxidation phase when the fuel oxygen potential is low. Then, after clad oxidation, significant fuel oxidation occurs, sufficient for total transfer of Mo out of the metallic phase, under oxides forms. Significant part of these oxides are released through interconnected porosities but another part form molybdates with Ba an Sr only, because Cs is considerably released during clad oxidation phase. These molybdates remain stable during the final oxidising part of the experiment.

It is worth noting that this scenario is in agreement with recent Electron Probe Micro Analysis of metallic phases and dot mapping performed on samples located at high elevation, where temperature did not exceed 2300 K, showing total removing of Mo from metallic inclusions and strong association with Ba notably.

4. Conclusions

The present paper briefly describes the models of the MFPR code and provides examples of the code applications to different regimes that a nuclear fuel may undergo. Models are based on self-consistent consideration of evolution of various point defects (gas atoms, vacancies and interstitials) and extended defects (gas bubbles, dislocations, vacancy clusters and pores) and their mutual interactions under various irradiation and annealing regimes of UO_2 fuel operation. Concerning chemically-active elements, the mechanistic approach of MFPR is based on complex association of a diffusion–vaporisation mechanism involving multi-phase and multi-component equilibrium at the grain boundary in association with accurate calculation of fuel oxidation.

The applications have shown the possibilities of the code in various situations and permit to define items for future developments. Among them, the model extension toward high burn-up and MOX fuel, the MFPR code coupling with thermo-mechanical fuel rod models, in order, notably, to take into account the strong interaction with the mechanical characteristics of the fuel, are foreseen.

For chemically active elements, the models will be improved by considering new separate phases and by including reaction kinetics between phases.

References

[1] M.S. Veshchunov, V.D. Ozrin, V.E. Shestak, V.I. Tarasov, R. Dubourg, G. Nicaise, Nucl. Eng. Des. 236 (2006) 179.
[2] R. Dubourg, H. Faure-Geors, G. Nicaise, M. Barachin, Nucl. Eng. Des. 235 (2005) 2183.

[3] G. Ducros, P.P. Malgouyres, M. Kissane, D. Boulaud, M. Durin, Nucl. Eng. Des. 208 (2001) 191.
[4] H. Kleykamp, J. Nucl. Mater. 131 (1985) 221.
[5] S. Imoto, J. Nucl. Mater. 140 (1986) 1927.
[6] E.H.P. Cordfunke, R.J.M. Konings, J. Nucl. Mater. 152 (1988) 301.
[7] E.H.P. Cordfunke, R.J.M. Konings, J. Nucl. Mater. 201 (1993) 57.
[8] K. Moriyama, H. Furuya, J. Nucl. Sci. Technol. 34 (1997) 900.
[9] T.B. Lindemer, T.M. Besmann, J. Nucl. Mater. 130 (1985) 473.
[10] M.S. Veshchunov, J. Nucl. Mater. 346 (2005) 208, 220.
[11] A.D. Brailsford, R. Bullough, Philos. Trans. Royal Soc. A 302 (1981) 87.
[12] M.S. Veshchunov, V.D. Ozrin, V.E. Shestak, V.I. Tarasov, R. Dubourg, G. Nicaise, in: Proceedings of 2004 International Meeting on LWR Fuel Performance, American Nuclear Society, Orlando, Florida, USA, September 19–22, 2004.
[13] R.J. White, M.O. Tucker, J. Nucl. Mater. 118 (1983) 1.
[14] S. Kashibe, K. Une, J. Nucl. Sci. Technol. 27 (1990) 1002.
[15] Ya.E. Geguzin, M.A. Krivoglaz, The Movement of Microscopic Inclusions in Solid State, Metallurgiya, Moscow, 1971.
[16] I. Zacharie, S. Lansiart, P. Combette, M. Trotabas, M. Coster, M. Groos, J. Nucl. Mater. 255 (1998) 85.
[17] K. Nogita, K. Une, Nucl. Instrum. and Meth. B 91 (1994) 301.
[18] S. Kashibe, K. Une, J. Nucl. Mater. 206 (1993) 22.
[19] J. Noirot, L. Noirot, L. Desgranges, L. Lamontagne, T. Baly, B. Pasquet, E. Muller, in: Proceedings of 2004 International Meeting on LWR Fuel Performance, American Nuclear Society, Orlando, Florida, USA, September 19–22, 2004.
[20] C. Baker, J. Nucl. Mater. 66 (1977) 283.
[21] J.A. Turnbull, R.M. Cornell, J. Nucl. Mater. 36 (1970) 161.
[22] M. Kinoshita, T. Sonoda, S. Kitajima, A. Sasahara, E. Kolstad, Hj. Matzke, V.V. Rondinella, A.D. Stalios, C.T. Walker, I.L.F. Ray, M. Sheindlin, D. Halton, C. Ronchi, in: ANS International Topical Meeting on LWR Fuel Behavior, Park City, Utah, USA, April 9–13, 2000.
[23] N. Hansen, D. Kuhlmann-Wilsdorf, Mater. Sci. Eng. 81 (1986) 141.
[24] A.D. Whapham, B.E. Sheldon, Electron Microscope Observation of the Fission-Gas Bubble Distribution in UO_2, AERE-R-4970, 1965.
[25] J.H. Evans, J. Nucl. Mater. 246 (1997) 121.
[26] Y. Pontillon, M.P. Ferroud-Plattet, D. Parrat, S. Ravel, G. Ducros, C. Struzik, I. Aubrun, G. Eminet, J. Lamontagne, in: Proceedings of 2004 International Meeting on LWR Fuel Performance, American Nuclear Society, Orlando, Florida, USA, September 19–22, 2004.